J Porous Mater (2016) 23:1037–1046
DOI 10.1007/s10934-016-0161-8

A facile synthesis route for modifying the catalytic performance of SAPO-18 in MTO process

Mohadese Nazari[1] · Reza M. Behbahani[2] · Gholamreza Moradi[1] · Alireza Samadi Lemraski[2]

Published online: 22 March 2016

Abstract In present work, a crystalline hierarchical SAPO-18 was synthesized using polyethylene glycol (PEG) as a cheap mesopore-directing agent to improve the catalytic performance in the methanol-to-olefin (MTO) process. The samples were characterized by XRD, FESEM, BET and NH_3-TPD analysis. The effect of PEG on the morphology, crystal size and crystallization time of catalyst was studied. The mesoporosity was tuned by varying the average molecular weight of PEG. Also, the influence of PEG MW on the textural and physicochemical properties of hierarchical SAPO-18 was investigated. Finally, the catalytic behavior of all the synthesized samples was evaluated for the MTO process at 698 K and atmospheric pressure with a feed WHSV of 2 h^{-1} in a fixed bed reactor. It was found that the presence of the multimodal pores in the SAPO-18 structure results in an increase of about 10 % in the light olefin selectivity. Micro-mesoporous SAPO-18 prepared by PEG4000 exhibited a high selectivity of 94 % to light olefins with a good stability of 12 h and the methanol conversion of 100 %.

Keywords Hierarchical SAPO-18 · Mesoporous · PEG · Methanol to olefin · Selectivity

✉ Gholamreza Moradi
gmoradi@razi.ac.ir

[1] Catalyst Research Center, Chemical Engineering Department, Faculty of Engineering, Razi University, Kermanshah 67149-67346, Iran

[2] Gas Engineering Department, Petroleum University of Technology, P.O. Box 63431, Ahvaz, Iran

1 Introduction

Light olefins are valuable intermediates for the petrochemical industry. In the recent decades, methanol-to-olefins (MTO) process has attracted interests as a promising route for the olefin production from non-oil sources. Silicoaluminophosphates with the appropriate structure and moderate acid strength have been introduced as the potential catalysts for this reaction [1]. Silicoaluminophosphate-18 is a small pore molecular sieve with a pore diameter of 3.8 × 3.8 Å. Tunable and weaker acid strength, larger cages and more rigid D6R arrangement in SAPO-18 have made it more resistant to coking than SAPO-34 [2–6]. However, the selectivity toward light olefins for this catalyst is less than that of reported for SAPO-34. So far, some work has been done on improving the catalytic performance of SAPO-18 for MTO reaction [6–9]. On the other hand, in the recent decade, several studies have suggested the fabrication of the multimodal porous structure in zeolites via double-templating synthesis approaches (soft or hard templates) to improve the catalytic performance [10, 11]. Soft templates are surfactants or long-chained polymers which are flexible under the synthesis conditions and react readily with the other components in the synthesis mixture [11]. They have the higher adaptability in tailoring the meso/macroporous structures than hard templates [12]. Polyethylene glycol (PEG) is a water-soluble linear polymer with a low toxicity, which can be utilized as an inexpensive soft template for preparation of hierarchical SAPOs [13–16]. Physical property and molecular weight of PEG are adjustable. Some studies have been done on the synthesis of the hierarchical SAPO-34 by PEG [13, 17], but to our knowledge, no paper has been reported on that of SAPO-18.

In the present work, we intend to synthesize the SAPO-18 catalyst with a hierarchical tuned structure via a one-

Table 1 Details of the synthesis conditions for the different samples

The samples	Average MW of PEG (g/mol)	Crystallization time (days)
SConv.(3)	–	3
S4000(3)	4000	3
S4000(5)	4000	5
S4000(7)	4000	7
S2000(5)	2000	5
S6000(5)	6000	5

step hydrothermal method using PEG as a mesopore-generating agent. The effect of PEG on the morphology, crystal size and crystallization time of catalyst was studied. The mesoporosity was also tuned by varying the average molecular weight of PEG. The influence of PEG MW on the textural and physicochemical properties of hierarchical SAPO-18 was investigated. Finally, the catalytic behavior of all the synthesized samples was in detail evaluated for the MTO process.

2 Experimental

2.1 Synthesis

Aluminum isopropoxide, phosphoric acid (85 wt%, aqueous solution), silica sol (40 wt% SiO_2), N,N-diisopropylethylamine and PEG (average molecular weight 2000, 4000 and 6000) were chosen as starting materials. The conventional SAPO-18 was prepared as previously described and was named SConv.(3) [5]. Also, the hierarchical SAPO-18s were synthesized with a molar composition of Al_2O_3:0.9P_2O_5:0.4SiO_2:1.6$C_8H_{19}N$:50H_2O:0.16PEG. Cui et al. [13] revealed that PEG/template mol ratio of 0.1 is optimum for MTO process in the synthesis of hierarchical SAPO-34. Therefore, this specific amount of PEG was dissolved in 40 ml deionized water, and 24.22 g of aluminum isopropoxide was then added to this mixture and stirred vigorously for several hours. 7.2 ml of phosphoric acid with 4 ml of deionized water were dropped under continuous stirring for 3 h. After being stirred for 1 h, the solution of 2.7 ml silica and 5.4 ml water was dropwise added to the solution and continued stirring for 1 h. Finally, 16.5 ml of the template was added gradually to the mixture. The resulting gel was allowed to be aged overnight under vigorous agitation at room temperature. The final solution was transferred into a 250 ml Teflon-lined stainless steel autoclave and was subjected to hydrothermal treatment at 433 K under autogenic pressure. The solid products were recovered by centrifugation, washed and then were dried in air overnight. The as-synthesized samples were calcined in air at 823 K for 6 h at the heating rate of 3 °C/min. Details of the synthesis conditions for the samples are given in Table 1.

2.2 Characterization and activity test

X-ray diffraction (XRD) was performed on an Equinox 3000 diffractometer (Inel, France) using CuKa radiation ($\lambda = 1.5418$ Å) operating at 35 kV and 20 mA. Field emission scanning electron microscope (FESEM) images were captured using a HITACHI S-4160 (China). Total surface area, pore volume and mesopore diameter distribution of the calcined samples were calculated by the Brunauer–Emmett–Teller (BET) and the Barrett–Joyner–Halenda (BJH) methods. Nitrogen adsorption and desorption isotherms were measured using a Micromeritics ASAP 2010 system at 77 K. Temperature-programmed desorption of ammonia (NH3-TPD) was conducted by a Pulse chemisorb 2705 apparatus equipped with a thermoconductivity detector. 0.2 g of sample was pretreated at 550 °C for 1 h and then cooled down to 100 °C under a dry He flow. The NH_3 gas stream was injected at the same temperature until adsorption saturation was reached. The sample was flushed with dry He to remove weakly adsorbed NH_3. Then the temperature was raised from 100 to 600 °C at a heating rate of 10 °C/min in the presence of helium flow.

2.3 Catalyst activity test

The catalytic reaction was performed at atmospheric pressure using a continuous downflow fixed bed microreactor with dimensions of 12 mm internal diameter and 20 cm length. A diagram of the reactor setup is schematically shown in Fig. 1. In this system, the aqueous methanol solution (methanol/water weight ratio of 4:1) was first injected by a dosing pump (0.01–9.99 ml/min) and evaporated by a pre-heater at 473 K. The gas feed was then directed to the reactor via a heat-traced tube. 2 g of the catalyst powder was diluted with quartz particles and loaded into the reactor. Previous to the reaction, the catalyst samples were pretreated under dry nitrogen flow at 723 K for 1.5 h. The reaction was carried out at the temperature of 698 K and constant weight hourly space velocity (WHSV) of 2 h^{-1}. A tube furnace was employed to heat up the

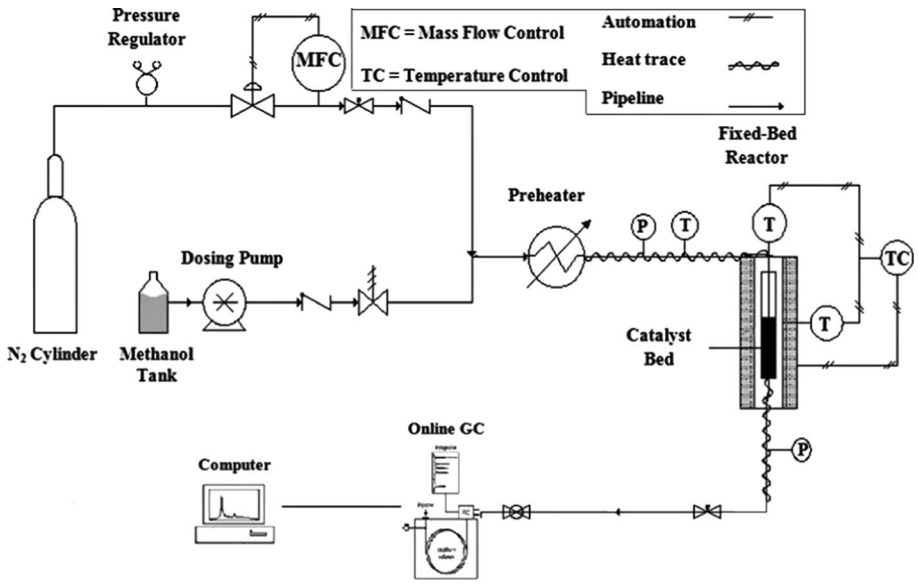

Fig. 1 The process flow diagram of the catalyst activity test setup

reactor to the desired operating temperature. Two thermocouples were inserted in the middle of the catalytic bed and the reactor wall. Reactor temperatures were controlled by a proportional-integral-derivative (PID) controller and recorded by the time during the test automatically. The gas-phase products were analyzed on-line by gas chromatography using an Agilent 6890 equipped with flame ionization detector (FID) and HP-PLOT Q column.

The methanol conversion and the products selectivity were calculated from the carbon number of species. The light olefin selectivity was defined as the ratio of the sum of produced ethylene, propylene, and butylene to all of the products. Also, the lifetime was defined as when light olefin selectivity began to drop down and the selectivity of dimethyl ether (DME) began to rise.

3 Results and discussion

3.1 Effect of PEG on the crystallization time

Three samples of hierarchical SAPO-18 were synthesized using PEG4000 in different crystallization times. The powder XRD patterns of the calcined samples exhibit characteristic reflections of SAPO-18 without any impurity phase and were in complete accordance with the simulated pattern of the AEI-type structure (Fig. 2). Characteristic peaks of S4000(3) with relatively low intensity imply that the sample mainly consists of very small crystallites along with the amorphous material. By prolonging the crystallization time to 5 days, the intensity of the peaks increases progressively and the amorphous phase almost disappears. The crystallinity reached the maximum level at 7 days.

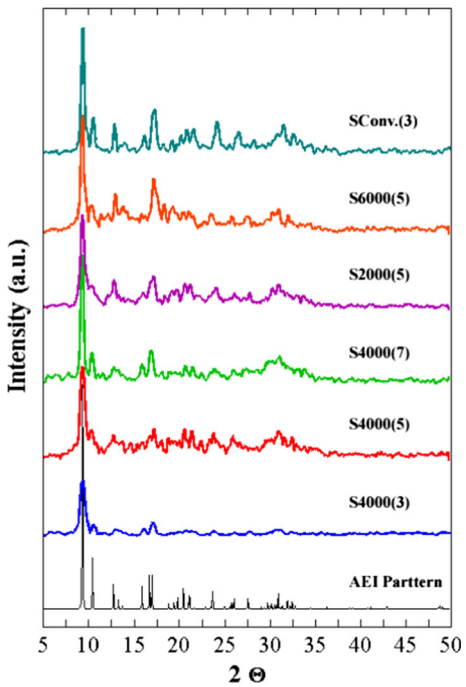

Fig. 2 XRD patterns of the synthesized hierarchical and conventional samples (AEI pattern is taken from IZA database [20])

Despite the fact that PEG can increase the nucleation rate by decreasing the surface tension and interfacial energy of the synthesis system [18, 19], the XRD results reveal that presence of PEG in the synthesis medium increases considerably the crystallization time of SAPO-18.

This can be due to the hydrogen bonding of ionic functional groups in PEG with silanol groups. These interactions possibly inhibit or decelerate the crystal growth via collision. Also, the functional groups coordinate

to aluminum ions and produce a stable complex as a bidentate ligand. These interactions reduce symmetry of the coordination structure of the aluminum cations, and would result in decreasing the crystallizability of its salt [14]. On the other hand, the addition of PEG increases solution viscosity and declines the transfer rate of the species and thus the growth rate of SAPO-18 crystals [19].

Figure 3 exhibits the evolution of the particles size and morphology of the hierarchical samples and compares them with the conventional SAPO-18. The relative size of the particles was measured using Image J software. The samples S4000(3), S4000(5), and S4000(7) show the average particle size of 80, 290, and 310 nm, respectively. Unlike the conventional SAPO-18 synthesized at 3 days which showed the good crystallinity with the average particle size of 240 nm [5], sample S4000(3) contains nanoparticles which coexisted with the amorphous phase. It suggests that addition of PEG into the synthesis solution can impressively limit the crystal growth. The figure also illustrates that PEG had no significant impact on the catalyst morphology.

The catalytic behavior of the samples was studied in MTO reaction. Figure 4a gives the methanol conversion and light olefin selectivity over the hierarchical catalysts versus time-on-stream. The results show that sample S4000(5) has the highest selectivity and the longest lifetime. Methanol conversion was over 99 % for all of the samples, however, S4000(3) deactivated rapidly at TOS of 5 h due to the low crystallinity and the presence of amorphous phase in its structure. S4000(7) also lost its activity after 7 h. It indicates the significant role of the particle and crystal sizes in the catalytic performance of the samples. The good crystallinity and small particles size of S4000(5) short diffusion length and lessen the polymerization reaction and thus, reduce considerably the rate of coke formation. Methane and DME selectivities are also depicted in Fig. 4b. The appearance of DME in the outlet stream is an indication of the beginning of catalyst deactivation. A higher $C_{2=}/C_{3=}$ ratio and a more methane yield were observed for S4000(5), except for when the catalyst was fresh.

The selectivities towards C_{5+} products and light alkanes are shown in Fig. 4c, d, respectively. Both figures show a relatively same declining trend. Alkanes and C_{5+} products are secondary products which are derived from primary products via hydrogen transfer reactions and are deeply influenced by two factors of acidity and diffusion path length [21]. Due to the presence of the strong acid sites on the surface of the fresh catalysts, the hydride transfer reaction is favorable and the selectivity towards the secondary byproducts is fairly high at the first hours of the reaction. A relatively high selectivity to light alkanes and C_{5+} for sample S4000(5) compared to S4000(7) can be possibly indicative of the presence of more Lewis acid or defect sites in the structure. As the reaction proceeds, most of the strong acid sites are quickly covered by coke species, and medium Brønsted acid sites become the predominant active sites of the catalyst. Therefore, light alkanes selectivity for samples S4000(2) and S4000(5) reduces close to zero and C_{5+} production (which mainly include aliphatic compounds) in a small amount remains constant during time on the stream and tends towards zero by deactivation

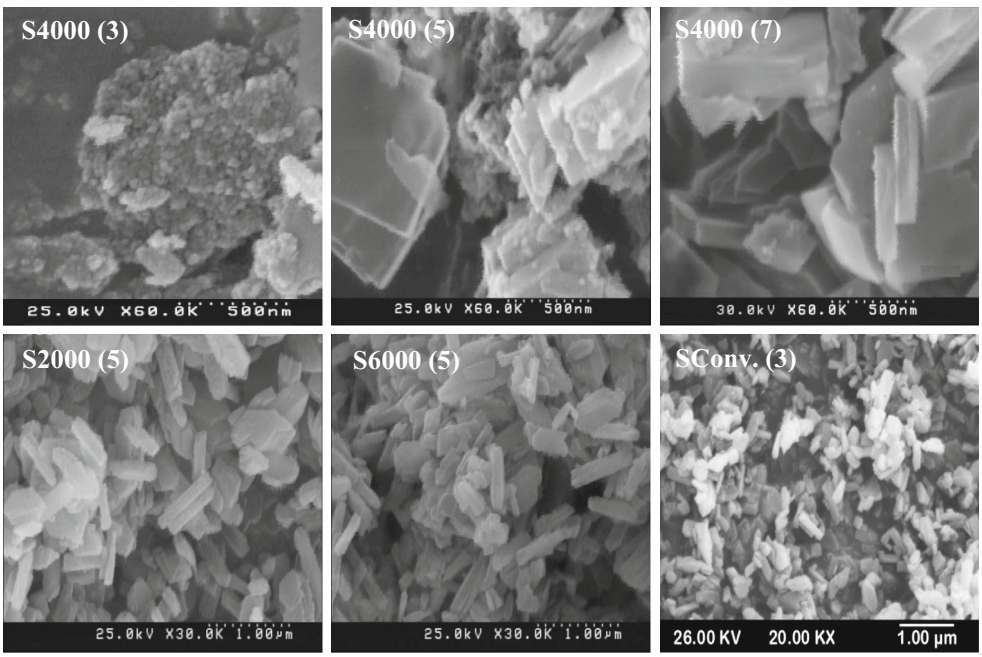

Fig. 3 SEM images of the synthesized catalysts (SEM image of sample SConve.(3) is taken from Ref. [5])

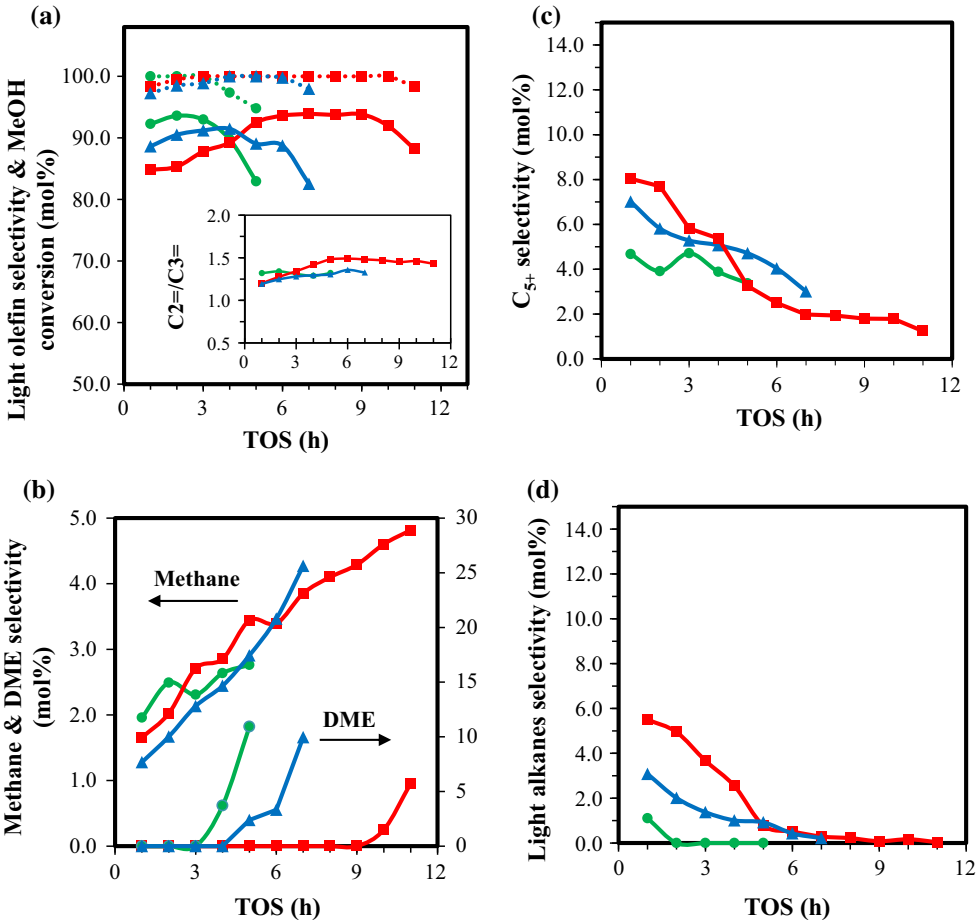

Fig. 4 **a** Light olefins selectivity (*solid lines*) and methanol conversion (*dot lines*), **b** methane and DME selectivities, **c** C_{5+} selectivity and **d** light alkanes selectivity of the samples prepared at different crystallization times: *circle* S4000(3), *square* S4000(5), *triangle* S4000(7)

of the Brønsted acid sites. However, this trend was different for sample S4000(7). The alkanes and C_{5+} byproducts are observed throughout the reaction with a declining trend. It can be because of the larger size of the particles and longer length of the diffusion path compared to other two catalysts, which results in more conversion of the olefins into alkane compounds along the diffusion path before leaving the catalyst surface and thus in a decrease in olefins selectivity. The results of catalytic test suggest that the optimum crystallization time for the synthesis of hierarchical SAPO-18 by PEG is about 5 days.

3.2 The effect of average molecular weight of PEG

To investigate influences of MW of PEG on structural and catalytic properties of hierarchical SAPO-18, two other samples of the catalysts were synthesized using PEG2000 and 6000 at 5 days. As is evident in Fig. 2, all the samples have the characteristic peaks of SAPO-18 crystalline phase. The impact of PEG MW on the XRD pattern of the hierarchical catalysts was negligible. The relative average particle size of samples S2000(5), S4000(5), and S6000(5) were 310, 290 and 340 nm, respectively. Also, SEM images illustrate that three samples are platelet-like particles and there was no obvious change in morphology and particle size (Fig. 3).

Acidic properties of the samples were investigated by NH_3-TPD analysis. All the catalysts demonstrate two distinct desorption peaks at about 160 and 360 °C, respectively (Fig. 5). The first peak is corresponding to P-OH hydroxyl groups and the second peak is indicative of strong Brønsted acid sites which are active sites for MTO process [22]. Total acidity values for samples of S2000(5), S4000(5), and S6000(5) were 0.825, 0.792, and 0.760 mmol/g respectively, which are much larger than that reported for the conventional SAPO-18 (0.570 mmol/g) [5]. It reveals that using PEG in the synthesis gel increases the acidity of SAPO-18. It could be because ether oxygens in PEG establish hydrogen-bonding interactions with silanol groups of silica sol and lead to high dispersion of Si into the aluminophosphate matrix. Dispersed silicons create more Brønsted acid sites than silicon islands [23]. It is observed that as PEG MW increases, the acidity is reduced. It may be due to the interaction of PEG molecules with each other. A long chain of high-MW PEG causes the molecule to coil around itself or to be spiraled with other

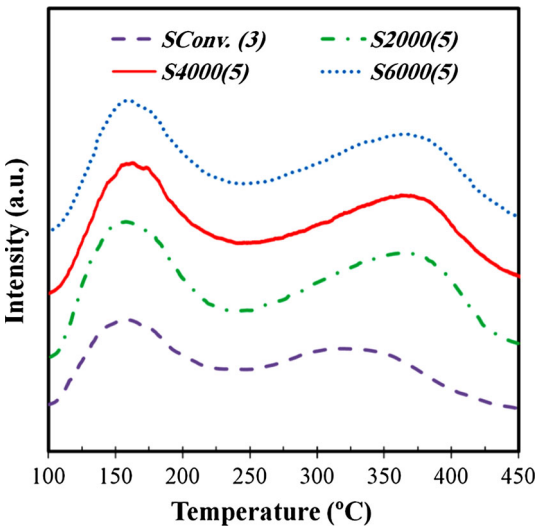

Fig. 5 TPD patterns of the conventional [5] and hierarchical SAPO-18s prepared by different MWs of PEG

PEG molecules through hydrogen bonding, that it decreases the number of effective PEG molecules that can interact with Si particles in the solution.

Nitrogen adsorption–desorption isotherms and the BJH pore size distribution plots obtained from the desorption branch are depicted in Fig. 6. According to IUPAC classification, the type IV isotherms with an H3-type hysteresis loop are observed for all the samples, which are corresponding to capillary condensation of the absorbate in the slit-shaped mesopores. Conventional SAPO-18 showed a very fast adsorption of nitrogen at $P/P_0 < 0.1$ indicating the presence of the micropores in the structure of the catalysts. As the relative pressure rose, a slight increase was observed in the adsorbed amount of nitrogen, whereas with adding PEG into the synthesis mixture and increasing its MW, a considerable increase was noticed in the absorbed volume and the hysteresis loop size. It suggests the presence of the meso/macropores in the structure of the catalysts prepared by PEG. All the pore size distribution plots show a common peak centered at about 3.5 nm which is caused by an abrupt desorption of nitrogen at a relative pressure of about 0.4. Therefore, this amount of the nitrogen desorbed at $P/P_0 \sim 0.4$ is attributed to not only the pores of 3.5 nm diameter but also to all mesopores with a diameter of less than 4 nm [24]. Peaks located at the range of 5–100 nm changes remarkably with increasing the MW PEG. Sample S4000(5) presents the mesoporous structure showing a large peak centered at 11 nm. S6000(5) exhibits a sharp increase in adsorption at P/P_0 of 0.9–1, indicating the

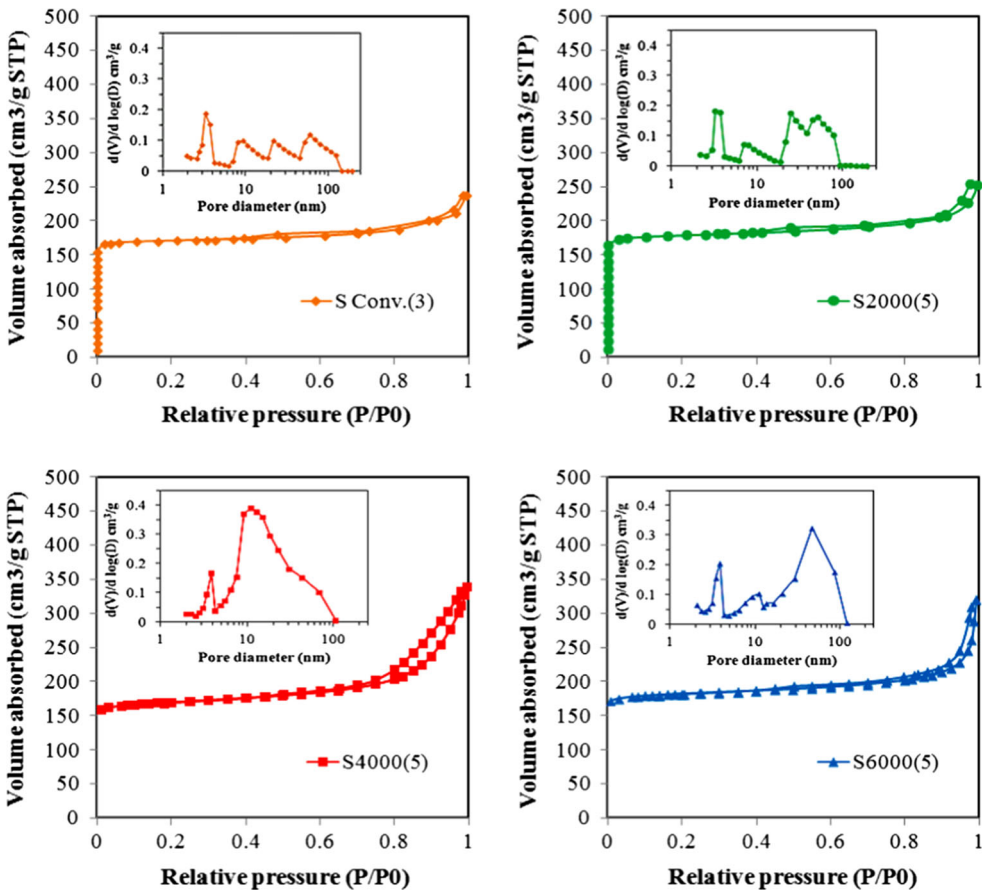

Fig. 6 N2 physisorption isotherms and BJH pore size distributions of the calcined samples

Table 2 Textural properties of the calcined samples

Sample	d_p[a] (nm)	S_{BET} (m^2/g)	S_{ext} (m^2/g)	V_{total} (cm^3/g)	V_{mic}[b] (cm^3/g)	BJH	
						d_p (nm)	V_{meso}
SConv.(3)	2	705	41	0.36	0.25	11.5	0.10
S2000(5)	2.1	723	48	0.38	0.26	11.6	0.12
S4000(5)	3.3	567	81	0.47	0.23	12.2	0.31
S6000(5)	2.5	607	67	0.38	0.25	13.3	0.25

[a] Adsorption average pore diameter ($4V_{total}/S_{BET}$)

[b] The micropore volumes determined by the t-plot method

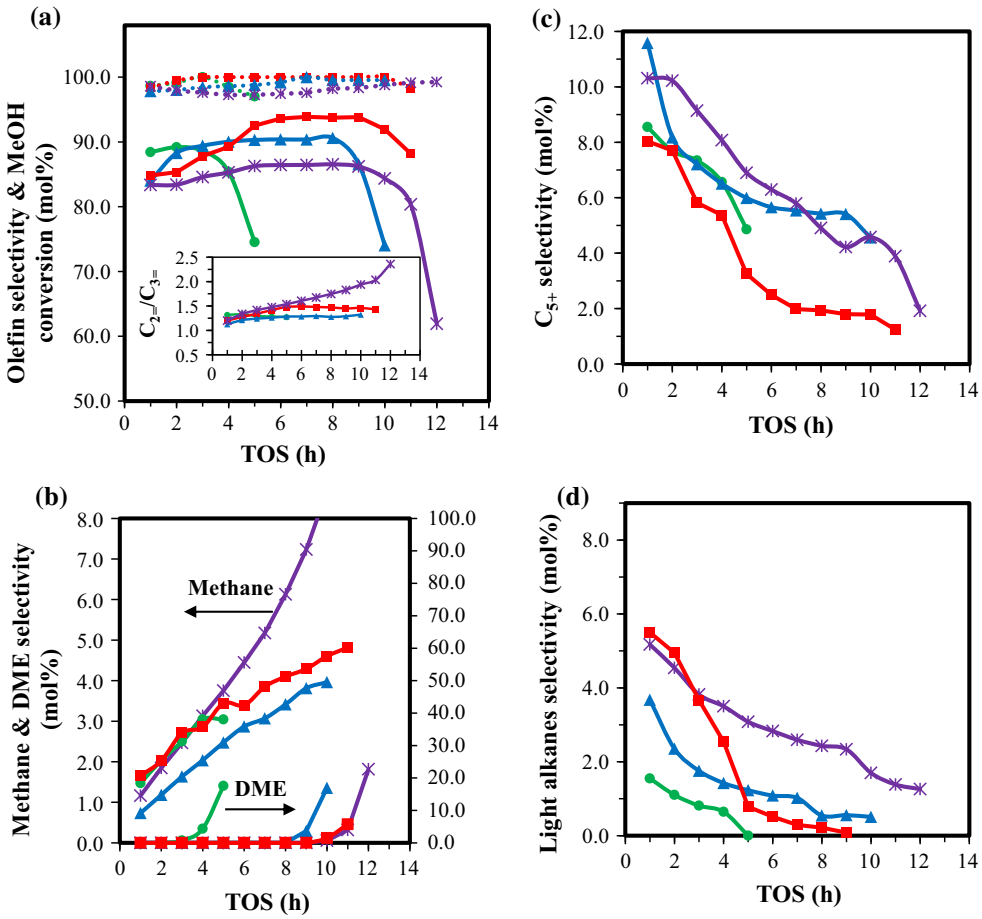

Fig. 7 **a** Light olefins selectivity (*solid lines*) and methanol conversion (*dot lines*), **b** methane and DME selectivities, **c** C_{5+} selectivity and **d** light alkanes selectivity of the samples prepared with different PEG MWs: *asterisk* SConv.(3) [5], *circle* S2000(5), *square* S4000(5), *triangle* S6000(5)

existence of macropores or interstitial voids in the structure. The peak shifted to a large pore range in its BJH plot confirms this result.

In fact, SAPO-18 crystal units are first formed via directing Si, Al, and P species by the template, and then are attracted to PEG through hydrogen-bonding with ethylene oxide groups. PEG trapped in the gel is encapsulated by SAPO crystals during hydrothermal treatment. Finally with removing the organic components by calcination, the desired micro/mesoporous structure is generated [13]. However, the pore size distribution exhibits that increasing PEG MW to 6000 resulted also in the formation of macropores. Two types of macropores can be distinguished in the structure: inter-crystalline and intra-crystalline. Inter-crystalline macropores are the spacing between nanocrystals, whereas Intra-crystalline macroporosity is induced in the network by phase separation. The phase separation process is expected to be enhanced with increasing PEG MW due to the increasing of the mixing free energy. Therefore, using PEG with high MW in the hierarchical SAPO-18 synthesis can amplify the presence of macropores within the framework.

Table 3 Comparison of the present hierarchical SAPO-18 with those reported on other hierarchical SAPO-34s and SAPO-18 in the literature

Catalysts	Additive	Operating conditions	MeOH Conversion	Olefin selectivity	Lifetime (min)[a]
SAPO-18	PEG 4000	T: 698 K WHSV: 2 h^{-1} MeOH:H_2O = 4:1 (wt ratio)	100 %	95 mol% (C_2–C_4)	720
SAPO-18 [8]	Chitosan	T: 673 K WHSV: 1.2 h^{-1} MeOH:N_2 = 1:1 (mol ratio)	100 %	92 mol% (C_2-C_4)	~600
SAPO-18 [8]	Carbon black particles	T: 673 K WHSV: 1.2 h^{-1} MeOH:N_2 = 1:1 (mol ratio)	100 %	92 mol% (C_2–C_4)	~420
SAPO-34 [17]	PEG2000	T: 723 K WHSV: 4 h^{-1} Feed: MeOH + Carrier gas	100 %	84.2 % (C_2–C_4)	~450
SAPO-34 [27]	Hydrofluoric acid	T: 673 K WHSV: 2 h^{-1} Feed: MeOH + N_2	100 %	84.8 % (C_2–C_3)	~600
SAPO-34 [28]	Quaternary ammonium-type organosilane	T: 723 K WHSV: 3 h^{-1} Feed: MeOH + Carrier gas	>99 %	81.16 % (C_2–C_3)	308
SAPO-34 [29]	Carbon nanotube	T: 743 K WHSV: 1 h^{-1} Feed: MeOH + He	100 %	~95 wt% (C_2–C_4)	310
SAPO-34 [29]	Carbon nanoparticle	T: 743 K WHSV: 1 h^{-1} Feed: MeOH + He	100 %	~95 wt% (C_2–C_4)	130

[a] Lifetime is defined as when catalyst activity began to drop down

Textural properties of the synthesized catalysts are summarized in Table 2. It can be seen that the incorporation of PEG into the gel increases mesopores volume and average pore diameter. The highest mesoporosity and the lowest micropore volume and surface area were observed for the sample prepared by PEG 4000.

The influence of PEG MW on the catalytic performance of SAPO-18 was investigated and compared to the results of conventional SAPO-18 reported in Ref. [5]. The trends of conversion and olefin selectivity as a function of TOS are depicted in Fig. 7a. All three hierarchical catalysts exhibit high activity (100 %), whereas this value was reported about 98–99 % for the conventional catalyst. Also, the hierarchical catalysts show an apparent increase in selectivity to light olefins. It can be explained by high acidity of the samples and facile transport of reactants and products through the intracrystalline mesopores. S4000(5) having the high mesoporosity in the structure affords the best selectivity (~94 %) which was about 10 % greater than the selectivity of the conventional SAPO-18. This catalyst has also the high durability like the conventional SAPO-18 despite having high acid density. It can be due to the facile and short diffusion pathway of coke precursors out of the crystal via mesopores. Figure 7a also shows $C_{2=}$/$C_{3=}$ ratio versus TOS. As seen from the figure, propylene production rises with increasing PEG MW. Light olefins are mainly derived from polymethyl benzenes entrapped in SAPO network. Propylene is produced from benzene molecules with four or more methyl groups [25]. Therefore, the presence of meso/macropores and channels in SAPO matrix favors production and diffusion of propylene. Methane selectivity has a direct relationship with the acidity of the catalyst and increases with increasing acidity in the hierarchical samples (Fig. 7b). Although the conventional SAPO-18 has less acidity than the hierarchical catalyst, the sole presence of micropores in its structure favors coke deposition and thus methane formation.

Figure 7c, d illustrate the selectivities to the alkanes and C_{5+} products. The conventional SAPO-18 having higher diffusion resistance produces more by-products (alkanes and C_{5+}) than the hierarchical SAPO-18s. Alkanes and C_{5+} products over this catalyst exhibit a slightly decrease trend throughout the reaction. As discussed in the previous section, strong acid sites and diffusion resistances are responsible for hydride transfer reactions producing the alkanes. The light olefins react to form paraffins, aromatics

and higher olefins by hydrogen transfer, alkylation and polycondensation during which they diffuse out of the SAPO pores. The presence of the significantly higher mesoporosity in the structure of sample S4000(5) compared other samples accelerates the escape of light olefins from the catalyst structure and decreases considerably the possibility of formation of the C_{5+} by-products. Due to the high external surface, sample S4000(5) includes a large number of strong Brønsted and Lewis acid sites in the structure. As found from Fig. 7d, in the first hours of the reaction, these strong acid sites favor the secondary reaction of olefins and produce more alkanes in the effluent. However, they are covered by coke formation after only a few hours, while the medium acid sites are still active. Therefore, deactivation of strong acid sites on the one hand, and short diffusion path in the mesoporous structure of catalyst S4000(5) on the other hand, decrease light alkane production close to zero and increase the light olefin selectivity.

As discussed in introduction section, SAPO-18 has inherent potentials which give supremacy to it over SAPO-34. But as reported in some work [3, 26], it shows lower olefin selectivity than SAPO-34 in MTO process. In present work, we prepared a new crystalline hierarchical SAPO-18 via an economic and facile route and enhance the catalytic performance by modifying the structural and chemical properties of the catalyst. The hierarchical SAPO-18 shows a superior performance with an increase of 10 % in olefin selectivity compared to conventional SAPO-18. For comparison purpose, the performance results reported for other hierarchical SAPO-18s and SAPO-34s are given in Table 3. It is found from the table, the hierarchical SAPO-18 synthesized by PEG 4000 presenting a superior catalytic performance can be considered as a desirable catalyst in MTO reaction.

4 Conclusions

A crystalline hierarchical SAPO-18 was successfully synthesized using PEG as a cheap mesopore-generating template. The effect of PEG on the crystallization time was investigated. It was found that using PEG in the synthesis gel reduces the crystallinity and crystal growth rate of SAPO-18. A crystallization time of 5 days was suggested as the most appropriate time for hydrothermal treatment of the hierarchical SAPO-18. The results also indicate the significant effect of MW of PEG on the structure and behavior of the catalyst. It was observed that porosity of the SAPO structure can be easily tailored for MTO reaction by changing MW of PEG. MW had no apparent influence on morphology and size of particles, whereas changed acidity properties of the catalyst. The performance of the synthesized hierarchical SAPO-18s was also studied in MTO process at 698 K and atmospheric pressure with a feed WHSV of 2 h^{-1} in a fixed bed reactor. The results revealed that the light olefin selectivity for the hierarchical SAPO-18 is about 10 % greater than that of the conventional SAPO-18. The sample prepared by PEG4000, with high and well-defined mesoporosity (3-50 nm) gave the selectivity of 94 % and a useful lifetime of 12 h, showing a better performance than the hierarchical SAPO-34s reported in the literature.

References

1. M. Stocker, Microporous Mesoporous Mater. **29**, 3 (1999)
2. J. Chen, P.A. Wright, J.M. Thomas, S. Natarajan, L. Marchese, S.M. Bradley, G. Sankar, C.R.A. Catlow, P.L. Gai-Boyes, R.P. Townsend, C.M. Lok, J. Phys. Chem. **98**, 10216 (1994)
3. J. Chen, J.M. Thomas, P.A. Wright, R.P. Townsend, Catal. Lett. **28**, 241 (1994)
4. D.S. Wragg, D. Akporiaye, H. Fjellvåg, J. Catal. **279**, 397 (2011)
5. M. Nazari, G. Moradi, R.M. Behbahani, M. Ghavipour, S. Abdollahi, Catal. Lett. **145**, 1893 (2015)
6. M. Nazari, G. Moradi, R.M. Behbahani, M. Ghavipour, J. Nat. Gas Sci. Eng. **29**, 337 (2016)
7. S. Abdollahi, M. Ghavipour, M. Nazari, R.M. Behbahani, G.R. Moradi, J. Nat. Gas Sci. Eng. **22**, 245 (2015)
8. T. Álvaro-Muñoz, C. Márquez-Álvarez, E. Sastre, Top. Catal. **59**, 278 (2016)
9. Q. Sun, Y. Ma, N. Wang, X. Li, D. Xi, J. Xu, F. Deng, K.B. Yoon, P. Oleynikov, O. Terasaki, J. Yu, J. Mater. Chem. A **2**, 17828 (2014)
10. C.M.A. Parlett, K. Wilson, A.F. Lee, Chem. Soc. Rev. **42**, 3876 (2013)
11. L.-H. Chen, X.-Y. Li, J.C. Rooke, Y.-H. Zhang, X.-Y. Yang, Y. Tang, F.-S. Xiao, B.-L. Su, J. Mater. Chem. **22**, 17381 (2012)
12. K. Na, M. Choi, R. Ryoo, Microporous Mesoporous Mater. **166**, 3 (2013)
13. Y. Cui, Q. Zhang, J. He, Y. Wang, F. Wei, Particuology **11**, 468 (2013)
14. M. Yabuki, R. Takahashi, S. Sato, T. Sodesawa, K. Ogura, Phys. Chem. Chem. Phys. **4**, 4830 (2002)
15. Y.W. Sun, Y.J. Wang, W. Guo, T. Wang, G.S. Luo, Microporous Mesoporous Mater. **88**, 31 (2006)
16. M. Razavian, S. Fatemi, Zeitschrift Für Anorg. Und Allg. Chemie **640**, 1855 (2014)
17. Q. Sun, N. Wang, G. Guo, X. Chen, J. Yu, J. Mater. Chem. A. **3**, 19783 (2015)
18. J. Yao, Y. Huang, H. Wang, J. Mater. Chem. **20**, 9827 (2010)
19. H. Sun, B. Shen, Adsorption **18**, 103 (2012)
20. http://www.iza-structure.org/databases
21. R.D. Cortright, J.A. Dumesic, Adv. Catal. **46**, 161 (2001)
22. L. Ye, F. Cao, W. Ying, D. Fang, Q. Sun, J. Porous Mater. **18**, 225 (2010)
23. G. Sastre, D.W. Lewis, C.R.A. Catlow, J. Phys. Chem. B **101**, 5249 (1997)
24. A.H. Janssen, A.J. Koster, K.P. De Jong, Mol. Cell **106**, 11905 (2002)
25. W. Song, H. Fu, J.F. Haw, J. Phys. Chem. B **105**, 12839 (2001)
26. J. Chen, P.A. Wright, S. Natarajan, J.M. Thomas, Stud. Surf. Sci. Catal. **84**, 1731 (1994)

27. D. Xi, Q. Sun, J. Xu, M. Cho, H.S. Cho, S. Asahina, Y. Li, F. Deng, O. Terasaki, J. Yu, J. Mater. Chem. A **2**, 17994 (2014)
28. C. Wang, M. Yang, P. Tian, S. Xu, Y. Yang, D. Wang, Y. Yuan, Z. Liu, J. Mater. Chem. A **3**, 5608 (2015)
29. F. Schmidt, S. Paasch, E. Brunner, S. Kaskel, Microporous Mesoporous Mater. **164**, 214 (2012)